Supplemental Data

Warfarin and vitamin K epoxide reductase: a molecular accounting for observed inhibition

Sangwook Wu[1,3,4], Xuejie Chen[2,4], Da-Yun Jin[2], Darrel W. Stafford[2],

Lee G. Pedersen[3*] & Jian-Ke Tie[2*]

[1]Department of Physics, Pukyong National University, Busan, 608-737, South Korea

[2]Department of Biology, University of North Carolina at Chapel Hill, Chapel Hill, NC 27599, USA

[3]Department of Chemistry, University of North Carolina at Chapel Hill, Chapel Hill, NC 27599, USA

[4]These authors contributed equally to this work

*Correspondence should be addressed to:

Lee G. Pedersen	OR	Jian-Ke Tie
Department of Chemistry		Department of Biology
University of North Carolina at Chapel Hill		University of North Carolina at Chapel Hill
Chapel Hill, NC 27599, USA		Chapel Hill, NC 27599, USA
Tel: 919-962-1578		Tel: 919-962-2267
E-mail: lee_pedersen@unc.edu		E-mail: jktie@email.unc.edu

The Supplemental Data includes:

Supplemental Figures 1 to 4

Supplemental Tables 1 to 3

Supplemental Note

Supplemental References

Supplemental Figures

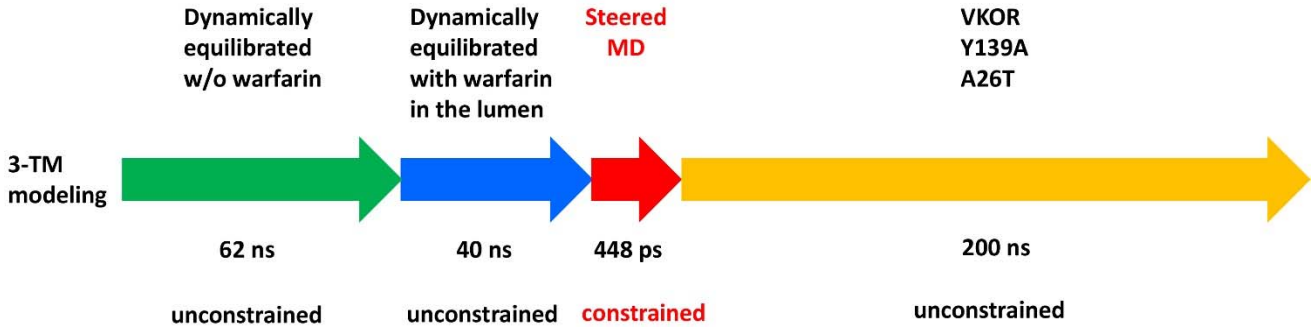

Supplemental Figure 1 Time profile of MD simulation of warfarin binding to VKOR.

Detailed information is provided in **Supplemental Table 1**.

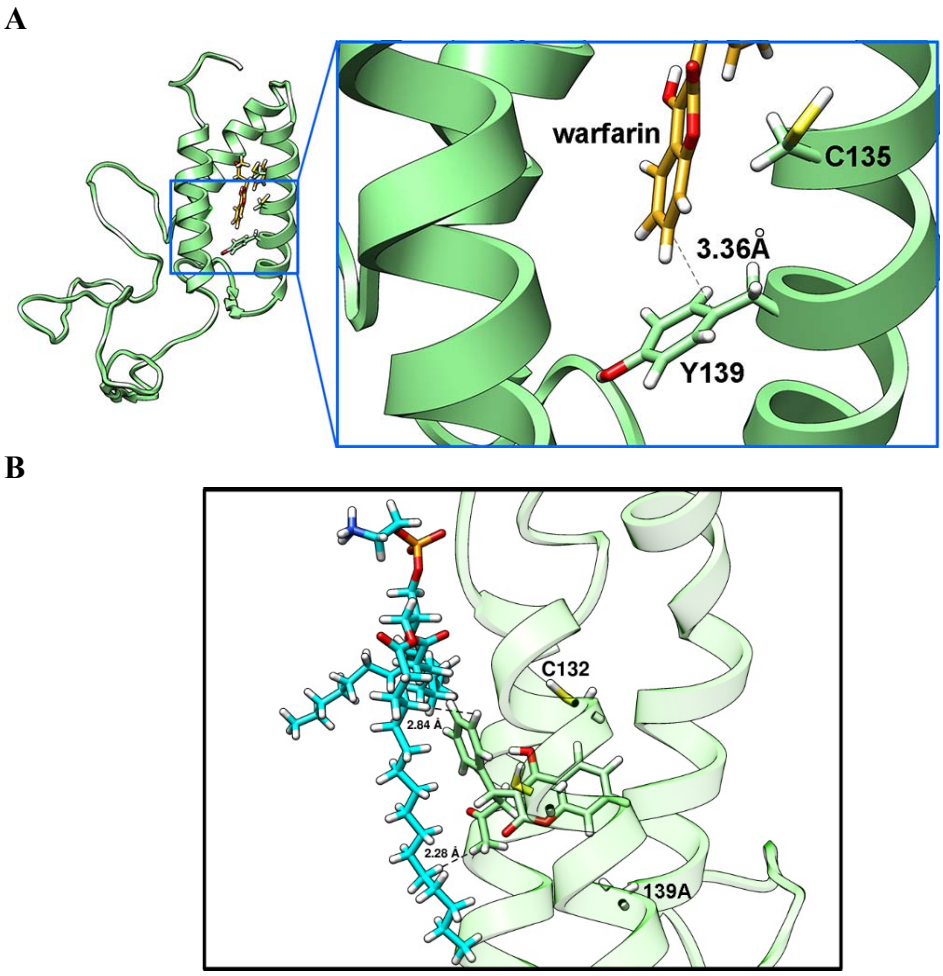

Supplemental Figure 2 Warfarin binds to wild-type and the Y139A mutant VKOR. (A) Warfarin forms a T-shaped π-π stacking interaction with residue Y139 (last snapshot of 448 ps steered MD simulation). The nearest carbon-carbon distance of 3.36 Å between warfarin and residue Y139 is labeled. Residues C135 and Y139 are labeled and displayed by stick diagrams. **(B)** Warfarin drifts away from the binding pocket of the Y139A mutant and interacts with a POPE lipid molecule in the environment. The snapshot is the same as in **Fig.4C**, it is rotated for effective viewing of the POPE lipid molecule. The lipid molecule that is nearst to warfarin is shown (carbon: cyan; hydrogen: white; oxygen: red; phosphate: gold; and nitrogen: blue).

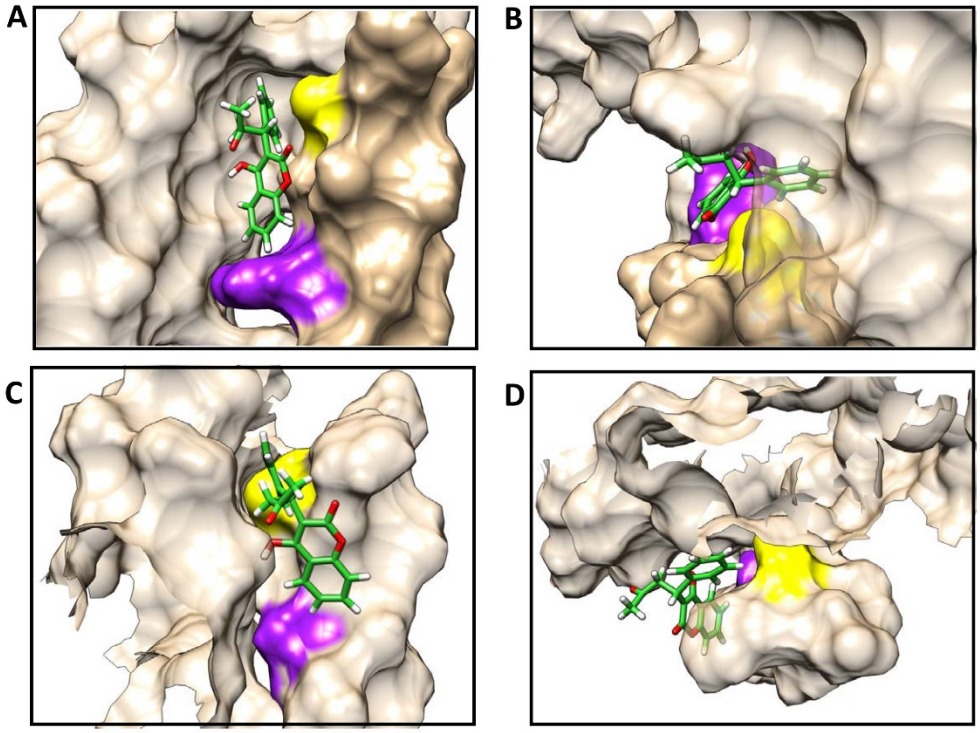

Supplemental Figure 3 The surface representation of warfarin-binding pocket for VKOR and the Y139A mutant. The surface representation of binding pocket for VKOR (**A,** top view; **B,** side view) and the Y139A mutant (**C**, top view; **D**, side view) at the last snapshot of the 200 ns unconstrained MD simulation. Reisdue 139 is highlighted in purple and C132 is higlighted in yellow. For the Y139A mutant, the binding pocket is closed and warfarin is outside of the binding pocket.

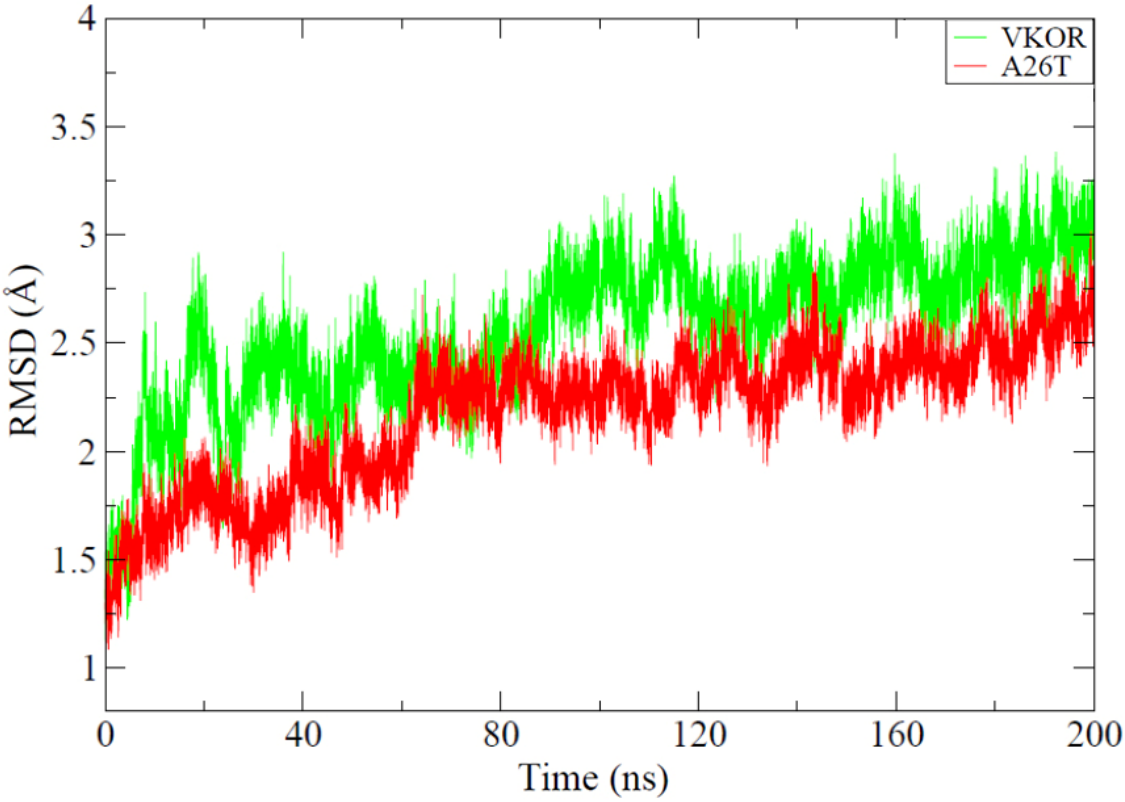

Supplemental Figure 4 Unconstrained conventional MD simulation of warfarin binding to VKOR and the A26T mutant. The backbone RMSD profiles of wild-type VKOR (green curve) and the naturally occurring warfarin-resistant A26T mutant (red curve) during the 200 ns unconstrained MD simulation are shown.

Supplemental Tables

Supplemental Table 1 Pertinent details of the four time-steps MD simulation of warfarin binding to VKOR

Step 1	62 ns equilibration of three-TM VKOR in large lipid and solvent box as previously described[1].
Step 2	40 ns equilibration of warfarin in ER lumen near the entrance of path to access the center of VKOR. The R-structure of warfarin (CID54678486) was downloaded as structure-data format (.sdf) from the PubChem compound database. The sdf format was then converted into PDB format in GaussView[2]. The necessary force field parameters were generated for warfarin using a geometry-optimized structure of warfarin with CHARMM[3]. MD simulations were performed as previously described[1].
Step 3	Steered MD simulation[4] was used to move the center of mass of warfarin from its equilibrated luminal position in the direction of the S atom of C132. The forcing spring constant was set to 7.0 kcal/mol Å2 with a pulling velocity (v) of 0.05 Å/ps during 448 ps[5]. By the end of the steered MD simulation, warfarin is found to be embedded in such a manner that the aromatic ring of the benzopyran fragment of warfarin is in a T-shaped π-π interaction with the aromatic ring of Y139. VKOR, Y139A and A26T are equilibrated with warfarin at this location.
Step 4	The three systems created in Step 3 are subjected to 200 ns MD as previously described[1]. A separate calculation was started for VKOR at 80ns, with equilibration following warfarin removal.

Supplemental Table 2 Comparison of warfarin resistance of VKOR mutants used in this study

	IC_{50}, nM	**R**	**Fold increase**
VKOR	6.959 ± 0.66	0.9970	1.00
Y25A	168.9 ± 25.8	0.9879	24.3
A26T	9.493 ± 1.51	0.9928	1.36
W59A	89.07 ± 10.8	0.9947	12.8
F55A	4045 ± 506	0.9947	581
F63A	174.3 ± 17.3	0.9967	25.1
Y139A	1975 ± 399	0.9803	284

Warfarin resistance is evaluated by determining the half-maximal inhibition concentration (IC_{50}) of warfarin for the wild-type VKOR and each of the VKOR mutants using cell-based activity assay. **IC_{50}** is calculated by GraphPad software. **R**: correlation coefficient.

Supplemental Table 3 Naturally occurring warfarin-resistant VKOR mutations[6-8]

AA Position	Mutation	Species	AA Position	Mutation	Species	AA Position	Mutation	Species
12	R12W	Mouse	52	S52W	Human	77	N77S	Human
25	Y25F	Rat		S52L	Human		N77Y	Human
26	A26T	Human/Rat/mouse	54	V54L	Human	90	I90L	Rat
	A26P	Human	56	S56F	Human	112	V112L	Rat
	A26S	Mouse		S56P	Rat	120	L120Q	Rat
27	L27V	Human	58	R58G	Human/Mouse	123	I123N	Human
28	H28Q	Human	59	W59C	Human	124	L124M	Mouse
29	V29L	Human		W59G	Mouse	128	L128R	Human
33	R33P	Rat		W59L	Human		L128N	Rat
34	A34P	Human		W59R	Human/Rat		L128Q	Rat
35	R35P	Rat		W59S	Mouse		L128S	Mouse
36	D36Y	Human	61	R61L	Mouse	139	Y139H	Human
	D36G	Human		R61W	Rat		Y139C	Human/Rat/Mouse
37	E37G	Mouse	63	F63C	Rat		Y139F	Rat
39	Y39N	Rat	66	V66M	Human		Y139S	Rat
41	A41S	Human		V66G	Human	141	I141V	Rat
	A41V	Rat	67	E67K	Rat	143	A143V	Rat
45	V45A	Human	71	G71A	Human			
48	A48T	Mouse	76	L76P	Rat			

Supplemental Note

Validation of the VKOR antibody

The VKOR antibody used in this study for immunofluorescence confocal imaging is an affinity purified rabbit polyclonal antibody that specifically recognizes the loop sequence of A34-W59 (which has a disputed ER location in the 3- and 4-TM topological models) of human VKOR. This antibody was validated for immunostaining of human VKOR in 51 cell types, and validated for protein array that shows a single peak corresponding to interaction only with its own antigen by The Human Protein Atlas (https://www.proteinatlas.org/ENSG00000167397-VKORC1/antibody). It was also validated for immunohistochemistry and for western blot analysis by ThermoFisher Scientific (https://assets.thermofisher.com/TFS-Assets/LSG/certificate/Certificates-of-Analysis/SD2373082_PA560093.pdf), where we purchased the antibody.

To further validate the VKOR antibody in this study, whole cell lysates of HEK293 cells and HEK293 cells with their endogenous VKOR knocked out were used for western blot analysis. GAPDH was used as a sample loading control. Our result shows that the VKOR antibody recognizes only a single band at ~18 kDa (Figure below, **Figure A**, lane 1), which is consistent with the apparent molecular weight of human VKOR in SDS-PAGE[9]. Knockout of the VKOR gene in HEK293 cells abolished VKOR protein expression (Figure below, **Figure A**, lane 2). These results agree with the validation data from The Human Protein Atlas and from ThermoFisher Scientific indicating that the VKOR antibody used in this study is specific for human VKOR.

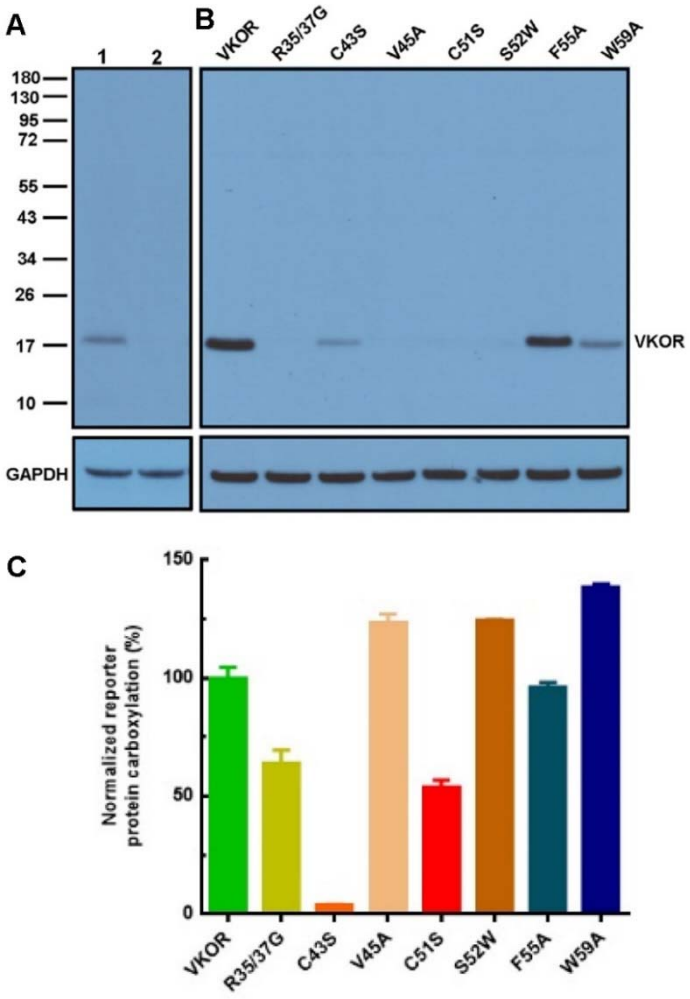

Validation of the VKOR antibody. (**A**) The whole cell lysate of HEK293 cells (lane 1) and HEK293 cells with their endogenous VKOR knocked out (lane 2) were used for western blot analysis to validate the VKOR antibody. (**B**) The wild-type VKOR and its various mutants in the corresponding loop sequence were transisently expressed in VKOR-deficient FIXgla-PC/HEK293 reporter cells. The cells were lysed 48 hours post-transfection and the whole lysate was used for western blot analysis. GAPDH: sample loading control. (**C**) The cell-based activity assay of VKOR and its mutants used in western blot analysis in (**B**). For details, please refer to Supplemental Note, validation of the VKOR antibody.

To further confirm that the VKOR antibody specifically recognizes the loop sequence (A34-W59) of human VKOR, we made a series of VKOR mutations within this loop sequence

(R35/37G, C43S, V45A, C51S, S52W, F55A, and W59A) and transiently expressed these mutations in FIXgla-PC/HEK293 reporter cells with their endogenous VKOR knocked out. The transfected cells were cultured with 5 μM KO for 48 hours. The cell culture medium was collected for cell-based VKOR activity assay, and the cell pellet was used for western blot validation of the VKOR antibody. Our results show that except for the F55A mutant, all other VKOR mutants have significantly decreased intensity of the VKOR protein band in western blot analysis (**Supplemental Figure 2B**). It appears that the decreased intensity of the VKOR protein band is not due to variations of VKOR protein expression levels, as these mutants have reasonable VKOR activities, except for the C43S mutant (**Supplemental Figure. 2C**). The abolished VKOR activity of the C43S mutant appears not related to the diminished VKOR protein band in western blot, as the C43S mutant has a similar protein expression level as the wild-type VKOR when determined by their C-terminal FLAG tagged fusions[10]. Thus, these results suggest that the VKOR antibody used in this study is specific for human VKOR's loop sequence (A34-W59) which immediately follows TM1.

Modeling warfarin binding to active site reduced VKOR

Before the identification of VKOR, warfarin was proposed to preferentially bind to oxidized VKOR that had a disulfide-linked active site[11-13]. An *in vitro* DTT-driven activity study showed that warfarin inhibits VKOR more strongly when VKOR is pre-incubated with a higher concentration of KO, conditions presumed to produce more oxidized VKOR[12]. Recently, Shen *et al* reported that warfarin preferentially binds to VKOR with C51 (loop cysteine) and C132 (active site cysteine) linked by a disulfide bond[10], and that pre-incubation of VKOR in HEK293 cells with

KO significantly increased the intramolecular disulfide bond formation of VKOR. These authors show that over 95% of VKOR's active site cysteines (C132 and C135) and 80% of the loop cysteines (C43 and C51) are oxidized after 5 hours' incubation with KO. To examine how the redox status of VKOR's cysteines affects warfarin's inhibition of VKOR in its native milieu, we pre-incubated VKOR in HEK293 cells with KO for 5 and 24 hours, respectively. Warfarin resistance of KO treated and non-treated cells was examined. Our results show that increasing intramolecular disulfide bond formation by pre-incubating VKOR with KO does not affect warfarin binding (**Figure** below). Therefore, all of our MD simulations were performed using VKOR with its active site reduced. It should be noted that an oxidized active site (disulfide-linked C132 and C135) would not necessarily preclude warfarin binding in our model.

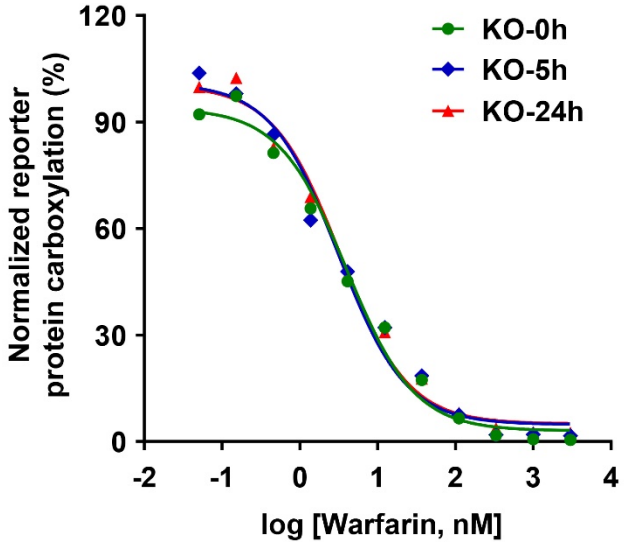

Effect of the redox status of VKOR's cysteines on warfarin inhibition. FIXgla-PC/HEK293 reporter cells were pre-incubated with 5 μM KO for 5 and 24 hours. Warfarin resistance was performed as described in **Figure 5**.

Modeling warfarin binding to VKOR via cytoplasm

Since the reduction of KO by VKOR and vitamin K-dependent carboxylation occur in the ER lumen, we performed MD simulation of warfarin binding to VKOR from the ER lumen. As a comparison, we also performed MD simulation of warfarin accessing its proposed binding site from the cytoplasm. For the steered MD simulation, we used a spring constant of 20.0 kcal/mol $Å^2$ and a pulling velocity of 0.05 Å/ps during a 904 ps simulation. Since we have to increase the spring constant, this implies that warfarin needs to overcome a higher energy barrier in order to approach its binding site. Even with an increased spring constant, our simulation results show that warfarin cannot access its binding site, as shown in the following figure.

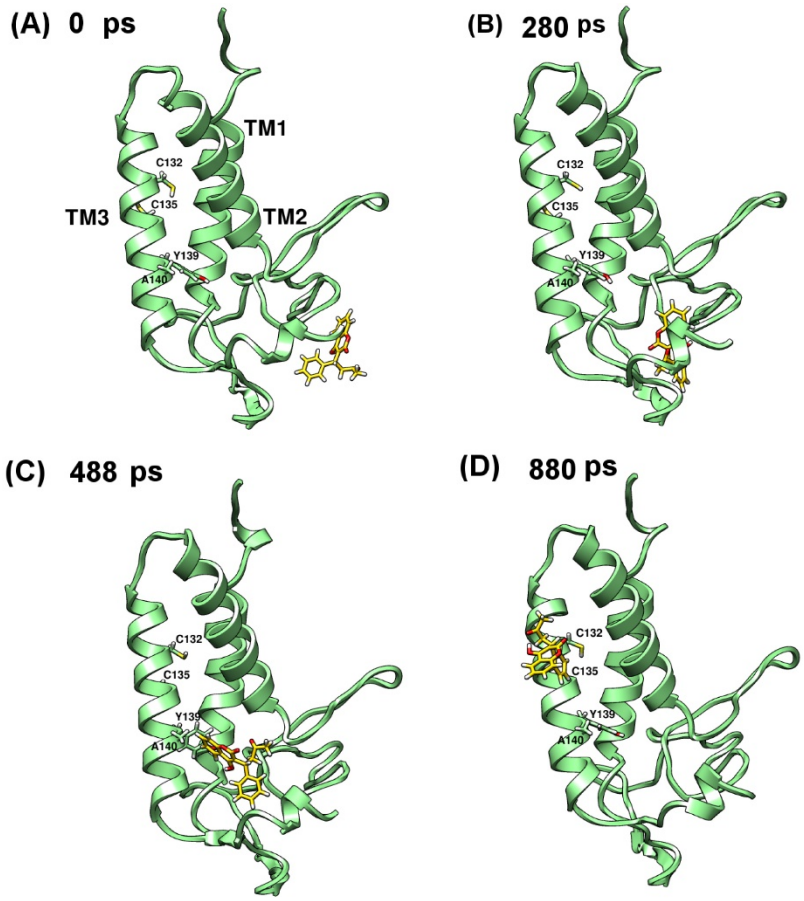

MD simulation of warfarin binding to VKOR from the cytoplasm.

Distinguish between reversible and irreversible inhibitions

Two mechanisms for warfarin's inhibition of VKOR have been proposed: reversible and irreversible[14,15]. Both types of inhibitions decrease Vmax at a fixed enzyme concentration. However, these two inhibition types can be distinguished by plotting Vmax versus different enzyme concentrations in the presence and absence of an inhibitor[16]. In the case of a reversible inhibition, the response of Vmax to enzyme concentration with inhibitor will have a smaller slope (**Figure** below, blue line) than the control (without inhibitor, green line), and the two curves will intersect at the origin. This applies to a reversible inhibitor that has a tight binding to the enzyme, such as warfarin binds VKOR[15,17]. In the case of an irreversible inhibition, the enzyme is inactivated until all of the irreversible inhibitor is used up. Thereafter, the enzyme has the same kinetics as that with no inhibitor. Therefore, the response of Vmax to enzyme concentration with irreversible inhibitor will have the same slope as the control (**Figure** below, red line), but it will

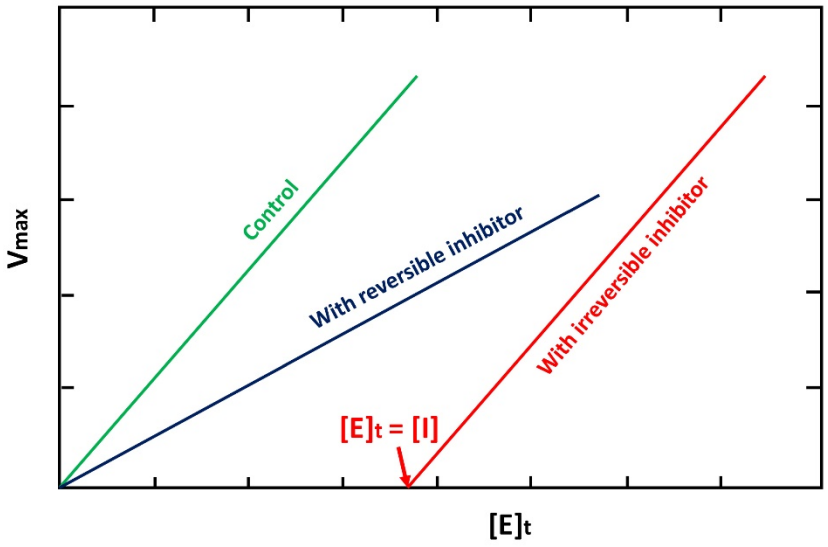

The response of Vmax to enzyme concentrations in the presence and absence of an irreversible or reversible inhibitor.

intersect the horizontal axis at a position equivalent to the concentration of the irreversible inhibitor—the concentration of enzyme that is irreversibly inactivated by the inhibitor.

In this study, the plotted lines of Vmax versus VKOR concentrations in the presence of warfarin have smaller slopes than the control line and intersect with the control line close to the origin (**Figure 5E**), suggesting a reversible inhibition mechanism of warfarin inhibition of VKOR.

The differences between human VKOR and its bacterial homologue

Since VKOR bacterial homologues (VKORHs) were identified as part of a disulfide bond formation pathway in bacteria[18], the structure and reaction mechanism of VKORH have been applied to human VKOR[19,20]. However, VKORHs and human VKOR appear to have very different biological functions and topological structures. Human VKOR's biological function is to reduce vitamin K epoxide (KO) to vitamin K to support vitamin K-dependent carboxylation. When KO is reduced to vitamin K, the reduced active site $C_{132}XXC_{135}$ of VKOR is oxidized to a disulfide. The oxidized active site must ultimately be reduced back to free cysteines for the enzyme to be active. Thus, the active form of human VKOR has a reduced $C_{132}XXC_{135}$ active site.

However, the biological function of VKORH is to promote protein oxidative folding in bacteria[18]. After an intramolecular disulfide of a nascent peptide is formed by the thiol-disulfide oxidoreductase (DsbA), DsbA transfers the reducing equivalents to a pair of VKORH's loop cysteines, then to its CXXC redox motif. This process reduces the oxidized (disulfide linked) CXXC redox motif to its reduced form. For the enzyme to become active, the reduced CXXC active site must ultimately be oxidized back to a disulfide by ubiquinone. Thus, the biologically

active form of VKORH has an oxidized CXXC active site, which is the opposite as human VKOR. Therefore, human VKOR and its bacterial homologues have different biological functions and active site redox status requirements; results with either group should be interpreted carefully when applied to the other.

Human VKOR and its bacterial homologue appear to also have different topological structures[21]. Most biochemical data accumulated from membrane topology studies of human VKOR support a three-TM topological structure[22-24], while the VKOR-like domain in VKORHs has four TM helices[18,20,25]. Topological structures for each of the individual proteins agree with most of the membrane protein topology determinants and with the results from the membrane topology prediction program TMHHM (**Figure** below). However, generalizing the four-TM topological structure of VKORH to human VKOR is the basis of the conflict.

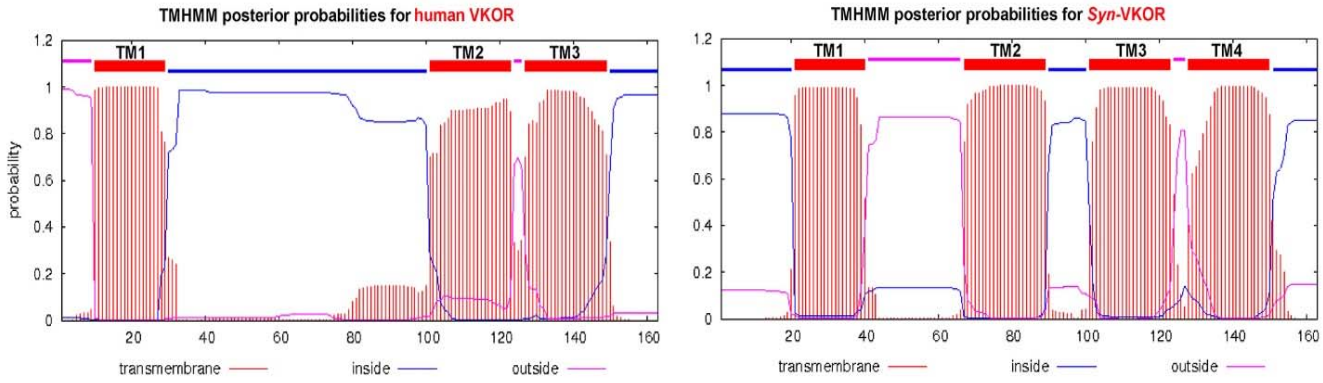

Membrane topology of human VKOR and *Syn*-VKOR predicted by TMHMM.
The VKOR-like domain of *Syn*-VKOR from residue 1-163 was used for prediction.

Supplemental References

1. Wu S, Tie JK, Stafford DW, Pedersen LG. Membrane topology for human vitamin K epoxide reductase. *J Thromb Haemost*. 2014;12(1):112-114.
2. Frisch MJ, Trucks GW, Schlegel HB, et al. Gaussian 03, Revision C.02. *Gaussian, Inc, Wallingford CT,* . 2004.
3. Brooks BR, Brooks CL, 3rd, Mackerell AD, Jr., et al. CHARMM: the biomolecular simulation program. *J Comput Chem*. 2009;30(10):1545-1614.
4. Phillips JC, Braun R, Wang W, et al. Scalable molecular dynamics with NAMD. *J Comput Chem*. 2005;26(16):1781-1802.
5. The PyMOL Molecular Graphics System, Version 1.2r3pre, Schrödinger, LLC.
6. Goulois J, Chapuzet A, Lambert V, et al. Evidence of a target resistance to antivitamin K rodenticides in the roof rat Rattus rattus: identification and characterisation of a novel Y25F mutation in the Vkorc1 gene. *Pest Manag Sci*. 2016;72(3):544-550.
7. Oldenburg J, Muller CR, Rost S, Watzka M, Bevans CG. Comparative genetics of warfarin resistance. *Hamostaseologie*. 2014;34(2):143-159.
8. Rost S, Pelz HJ, Menzel S, et al. Novel mutations in the VKORC1 gene of wild rats and mice--a response to 50 years of selection pressure by warfarin? *BMC Genet*. 2009;10:4.
9. Chu PH, Huang TY, Williams J, Stafford DW. Purified vitamin K epoxide reductase alone is sufficient for conversion of vitamin K epoxide to vitamin K and vitamin K to vitamin KH2. *Proc Natl Acad Sci U S A*. 2006;103(51):19308-19313.

10. Shen G, Cui W, Zhang H, et al. Warfarin traps human vitamin K epoxide reductase in an intermediate state during electron transfer. *Nat Struct Mol Biol*. 2017;24(1):69-76.

11. Silverman RB, Nandi DL. Reduced thioredoxin: a possible physiological cofactor for vitamin K epoxide reductase. Further support for an active site disulfide. *Biochem Biophys Res Commun*. 1988;155(3):1248-1254.

12. Fasco MJ, Principe LM, Walsh WA, Friedman PA. Warfarin inhibition of vitamin K 2,3-epoxide reductase in rat liver microsomes. *Biochemistry*. 1983;22(24):5655-5660.

13. Silverman RB. Chemical model studies for the mechanism of vitamin K epoxide reductase. *J Am Chem Soc*. 1981;103(19):5939-5941.

14. Lasseur R, Longin-Sauvageon C, Videmann B, Billeret M, Berny P, Benoit E. Warfarin resistance in a French strain of rats. *J Biochem Mol Toxicol*. 2005;19(6):379-385.

15. Fasco MJ, Principe LM. R- and S-Warfarin inhibition of vitamin K and vitamin K 2,3-epoxide reductase activities in the rat. *J Biol Chem*. 1982;257(9):4894-4901.

16. Segel IH. Enzyme Kinetics: Behavior and Analysis of Rapid Equilibrium and Steady-State Enzyme Systems. *Wiley-Interscience*. 1993.

17. Lorusso DJ, Suttie JW. Warfarin binding to microsomes isolated from normal and warfarin-resistant rat liver. *Mol Pharmacol*. 1972;8(2):197-203.

18. Dutton RJ, Boyd D, Berkmen M, Beckwith J. Bacterial species exhibit diversity in their mechanisms and capacity for protein disulfide bond formation. *Proc Natl Acad Sci U S A*. 2008;105(33):11933-11938.

19. Schulman S, Wang B, Li W, Rapoport TA. Vitamin K epoxide reductase prefers ER membrane-anchored thioredoxin-like redox partners. *Proc Natl Acad Sci U S A*. 2010;107(34):15027-15032.

20. Li W, Schulman S, Dutton RJ, Boyd D, Beckwith J, Rapoport TA. Structure of a bacterial homologue of vitamin K epoxide reductase. *Nature*. 2010;463(7280):507-512.

21. Tie JK, Jin DY, Stafford DW. Human vitamin K epoxide reductase and its bacterial homologue have different membrane topologies and reaction mechanisms. *J Biol Chem*. 2012;287(41):33945-33955.

22. Tie JK, Jin DY, Stafford DW. Conserved loop cysteines of vitamin K epoxide reductase complex subunit 1-like 1 (VKORC1L1) are involved in its active site regeneration. *J Biol Chem*. 2014;289(13):9396-9407.

23. Tie JK, Jin DY, Stafford DW. Mycobacterium tuberculosis vitamin K epoxide reductase homologue supports vitamin K-dependent carboxylation in mammalian cells. *Antioxid Redox Signal*. 2012;16(4):329-338.

24. Tie JK, Nicchitta C, von Heijne G, Stafford DW. Membrane topology mapping of vitamin K epoxide reductase by in vitro translation/cotranslocation. *J Biol Chem*. 2005;280(16):16410-16416.

25. Wang X, Dutton RJ, Beckwith J, Boyd D. Membrane topology and mutational analysis of Mycobacterium tuberculosis VKOR, a protein involved in disulfide bond formation and a homologue of human vitamin K epoxide reductase. *Antioxid Redox Signal*. 2011;14(8):1413-1420.